LIMNOLOGY
and
OCEANOGRAPHY

ASLO

Limnol. Oceanogr. 00, 2018, 00–00

doi: 10.1002/lno.10768

The physical limnology of a permanently ice-covered and chemically stratified Antarctic lake using high resolution spatial data from an autonomous underwater vehicle

Robert H. Spigel [1], **John C. Priscu,**[2] **Maciej K. Obryk,**[3] **William Stone,**[4] **Peter T. Doran**[3]*

[1]National Institute of Water and Atmospheric Research, Christchurch, New Zealand
[2]Department of Land Resources and Environmental Sciences, Montana State University, Bozeman, Montana
[3]Department of Geology and Geophysics, Louisiana State University, Baton Rouge, Louisiana
[4]Stone Aerospace, Del Valle, Texas

Abstract

We used an Environmentally Non-Disturbing Under-ice Robotic ANtarctic Explorer to make measurements of conductivity and temperature in Lake Bonney, a chemically stratified, permanently ice-covered Antarctic lake that abuts Taylor Glacier, an outlet glacier from the Polar Plateau. The lake is divided into two lobes – East Lobe Bonney (ELB) and West Lobe Bonney (WLB), each with unique temperature and salinity profiles. Most of our data were collected in November 2009 from WLB to examine the influence of the Taylor Glacier on the structure of the water column. Temperatures adjacent to the glacier face between 20 m and 22 m were 3°C colder than in the rest of WLB, due to latent heat transfer associated with melting of the submerged glacier face and inflow of cold brines that originate beneath the glacier. Melting of the glacier face into the salinity gradient below the chemocline generates a series of nearly horizontal intrusions into WLB that were previously documented in profiles measured with 3 cm vertical resolution in 1990–1991. WLB and ELB are connected by a narrow channel through which water can be exchanged over a shallow sill that controls the position of the chemocline in WLB. A complex exchange flow appears to exist through the narrows, driven by horizontal density gradients and melting at the glacier face. Superimposed on the exchange is a net west-to-east flow generated by the higher volume of meltwater inflows to WLB. Both of these processes can be expected to be enhanced in the future as more meltwater is produced.

Terrestrial perennially ice-covered aquatic environments of polar regions host vibrant, yet simple, microbial ecosystems that are mediated by the phenological responses of the ice covers (Bowman et al. 2016; Obryk et al. 2016). Small perturbations in the surface energy balance have been linked with ecosystem responses as a consequence of optical changes associated with the changing thickness of the ice covers (Obryk et al. 2016). Lakes in the McMurdo Dry Valleys of Antarctica are unique in that they have 3–6 m thick permanent ice covers and receive little stream flow, eliminating wind-mixing and reducing mixing caused by inflows. In addition, many of the lakes feature strong salinity gradients that control density stratification. Questions of the origin of these salts and why they have different compositions and concentrations among lakes are intimately connected with geological and geochemical evolution of the basins (e.g., Hendy et al. 1977; Poreda et al. 2004; Lyons et al. 2005; Doran et al. 2014).

Lake Bonney (Fig. 1), the focus of the present investigation, has been studied since the early 1960s (Armitage and House 1962). The first comprehensive evaluation of the physical limnology of the lake was done by Spigel and Priscu (1996, 1998) who made detailed microstructural measurements of temperature and conductivity to evaluate the stability of the water column and its influence on biological production. These authors attempted to examine the horizontal variation of these parameters in the lake, but logistics involved with drilling through the thick (3–5 m) ice limited the number of profiles that were feasible to make. Owing to these logistical constraints, vertical profiles of biogeophysical parameters in Lake Bonney since 1989 have been limited to annual measurements at a central index station located over the deepest part of the lake. Data from this location have been extrapolated across the horizontal extent of the lake, despite potential variation that may

*Correspondence: pdoran@lsu.edu

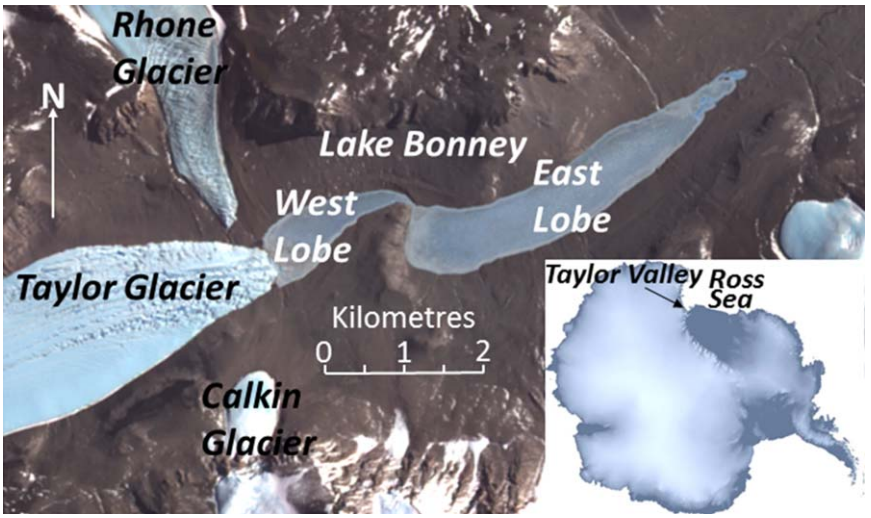

Fig. 1. Taylor Glacier terminus and Lake Bonney at the head of the Taylor Valley; underlying image from NASA's Visible Earth website (https://visibleearth.nasa.gov/view.php?id=35535). Inset shows location of the Taylor Valley in Antarctica (from https://visibleearth.nasa.gov/view.php?id=7624).

result from direct contact with the Taylor Glacier, an outlet glacier from the Polar Plateau.

We present results of a three-dimensional lake study using an autonomous underwater vehicle (AUV) named Environmentally Non-Disturbing Under-ice Robotic ANtarctic Explorer (ENDURANCE) that was deployed during the austral 2008/2009 and 2009/2010 summer field seasons. We examined specifically the influence of the submerged face of the Taylor Glacier and the exchange of water through the channel (the "narrows") that connects East Lobe Bonney (ELB) and West Lobe Bonney (WLB). A comparison is also made with data collected from low density manual profiling through individual drill holes in January 1991.

Methods

Details of the ENDURANCE, including the deployment, sample gridding, and navigational characteristics of the vehicle have been described previously (Stone et al. 2010; Obryk et al. 2014). Stone et al. (2010) also provide background information for the detailed mapping of the face of the Taylor Glacier and transects made through the channel connecting ELB and WLB.

Briefly, ENDURANCE was deployed through an $\sim$ 2 m diameter hole created in the perennial ice cover using standard drilling and melting techniques (Winslow et al. 2014). The vehicle executed a grid survey, with grid points being approximately 100 m apart (Fig. 2). At each grid point the vehicle would gently position itself against the underside of the ice and deploy the science package to profile the water column beneath, minimizing the disturbance of the stratified water column (Stone et al. 2010; Obryk et al. 2014). We used a laser altimeter to stop the sonde above the sediments, a measurement that was confirmed by on-board cameras.

Profiling with the AUV occurred from 10 December 2008 to 23 December 2008, and from 07 November 2009 to 02 December 2009. During 2008, an early melt season forced a shortened data collection confined to mostly the west end of WLB, so whole-basin comparisons in this paper use data from 2009 that were collected before the melt season. We focused on WLB and the narrows to investigate the influence of the Taylor Glacier on WLB and the exchange flow through the narrows into ELB.

Vertical profiles of conductivity, temperature, and pressure during the 2008 and 2009 field seasons were made using a SeaBird SBE 19plusV2 SEACAT Conductivity–Temperature–Depth (CTD) profiler sampling at 4 Hz and averaging two samples, resulting in a time interval of 0.5 s between data points. The CTD was deployed at drop speeds of $\sim$ 0.4 m s^{-1} from the ENDURANCE vehicle, resulting in a vertical distance between samples of $\sim$ 20 cm.

CTD data were also collected from November 1990 to January 1991 with a SeaBird SBE 25 Sealogger CTD deployed manually at drop speeds between 0.2 m s^{-1} and 0.3 m s^{-1} and sampling at 8 Hz; at a drop speed of 0.25 m s^{-1} this yielded a vertical distance of 3.1 cm between samples. This instrument and associated methods are described in detail in Spigel and Priscu (1996, 1998). Comparison tests between the SBE 19 and SBE 25 CTDs were conducted during the 2008–2009 summer season to ensure consistency between the measurements made by the two CTDs; the SBE25 is still in use in the McMurdo Dry Valleys Long Term Ecological Research project.

Measured and derived data obtained from the CTDs included temperature, practical salinity computed from conductivity, temperature, and pressure using UNSECO (EOS80) equations for seawater (Fofonoff and Millard 1983), and density at atmospheric pressure, computed from temperature

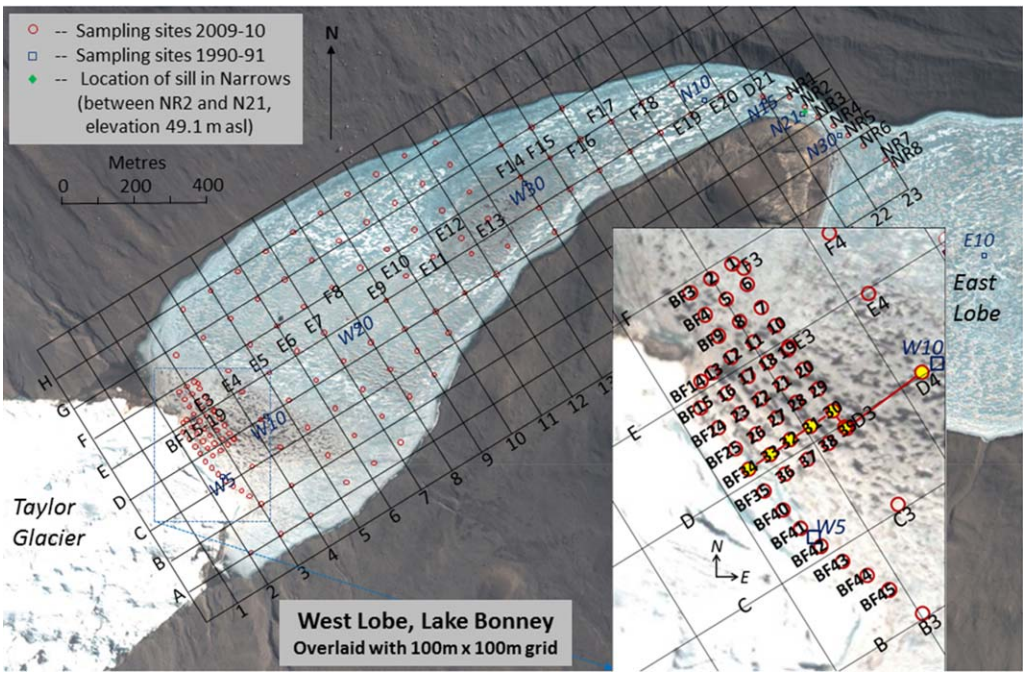

Fig. 2. Location map showing 100 m × 100 m sampling grid used for CTD profiling by ENDURANCE in WLB. Red circles mark locations where profiles were measured during 07 November 2009–24 November 2009; the labeled points are sites used in the west-east transect illustrated in Fig. 4. Sites occupied during a transect through the entire lake during 10 January 1991–11 January 1991 (Spigel and Priscu 1998) are shown by dark blue squares, with labels italicized. The inset shows the denser sampling grid near the front of the Taylor Glacier; location of sites used in the transect of Fig. 7 are highlighted in yellow and connected with red lines.

and salinity using UNESCO (EOS80) equations for seawater (Fofonoff and Millard 1983) as modified for the high salinities in Lake Bonney by Spigel and Priscu (1996). Density at atmospheric pressure was used because it closely approximates potential density over the depth range of Lake Bonney and is a good indicator of static stability (e.g., Phillips 1966, p. 13; Pond and Pickard 1978, p. 7).

We note that EOS80 was replaced in 2009 by the International Thermodynamic Equation of Seawater - 2010 (TEOS-10) as the International Oceanographic Commission's official description of seawater (*see*, e.g., http://salinometry.com/replacement-of-the-eos-80-definition-of-seawater-properties-with-teos-10/, posted October 2010, after the initial data processing for our study had been completed). Ideally TEOS-10 would have been used for data processing for the present paper. However, since the beginning of our studies on Lake Bonney in 1989, all measured CTD data have been processed using EOS80 equations for seawater, modified as described in Spigel and Priscu (1996) to allow calculation of salinity and density from the very high conductivities that characterize the deeper waters of both WLB and ELB. To ensure consistency with all of the historical data we felt it best to retain the same methodology for this paper as used in all of our work from 1989 to 2009.

Similarly, freezing-point temperatures corresponding to in situ values of salinity and pressure have been calculated using a formula of Millero and Leung (1976) based on experiments by Doherty and Kester (1974) and presented in Fofonoff and Millard (1983, p. 29). Fofonoff and Millard (1983) specify the range of salinities for application of the formula as $4 < S < 40$ PSU, which is a typical range for seawater. We have applied it to salinities up to 110 PSU (or greater), far beyond the range for which the formula was derived. However, comparison with the curve for NaCl solutions in the CRC Handbook of Chemistry and Physics (Lide 2005; *see* pp. 8–71 and pp. 8–116) implies that the extrapolation is reasonable. Temperature of maximum density as a function of pressure and salinity was calculated using the equation of Caldwell (1978).

All contour plots were drawn with Surfer version 11 (Golden Software 2012), using kriging for grid generation. It was necessary to specify a high degree of anisotropy when generating grids because of the extreme difference between gradients in the vertical compared to gradients in the horizontal. This was especially true for salinity and density.

Starting in 1999 water levels were recorded by a pressure transducer (Campbell Scientific CS-455, accuracy ± 0.1%) mounted on a buoy anchored on the lake bed. The sensor was mounted at approximately 10 m below the hydrostatic water surface (Winslow et al. 2014). Calibration for pressure-depth conversion was checked twice each year by manual lake level measurements using auto-levelling relative to fixed benchmarks on the lake shore. Between 1989 and 1999 manual water level readings were recorded, usually near the beginning and end of a field season.

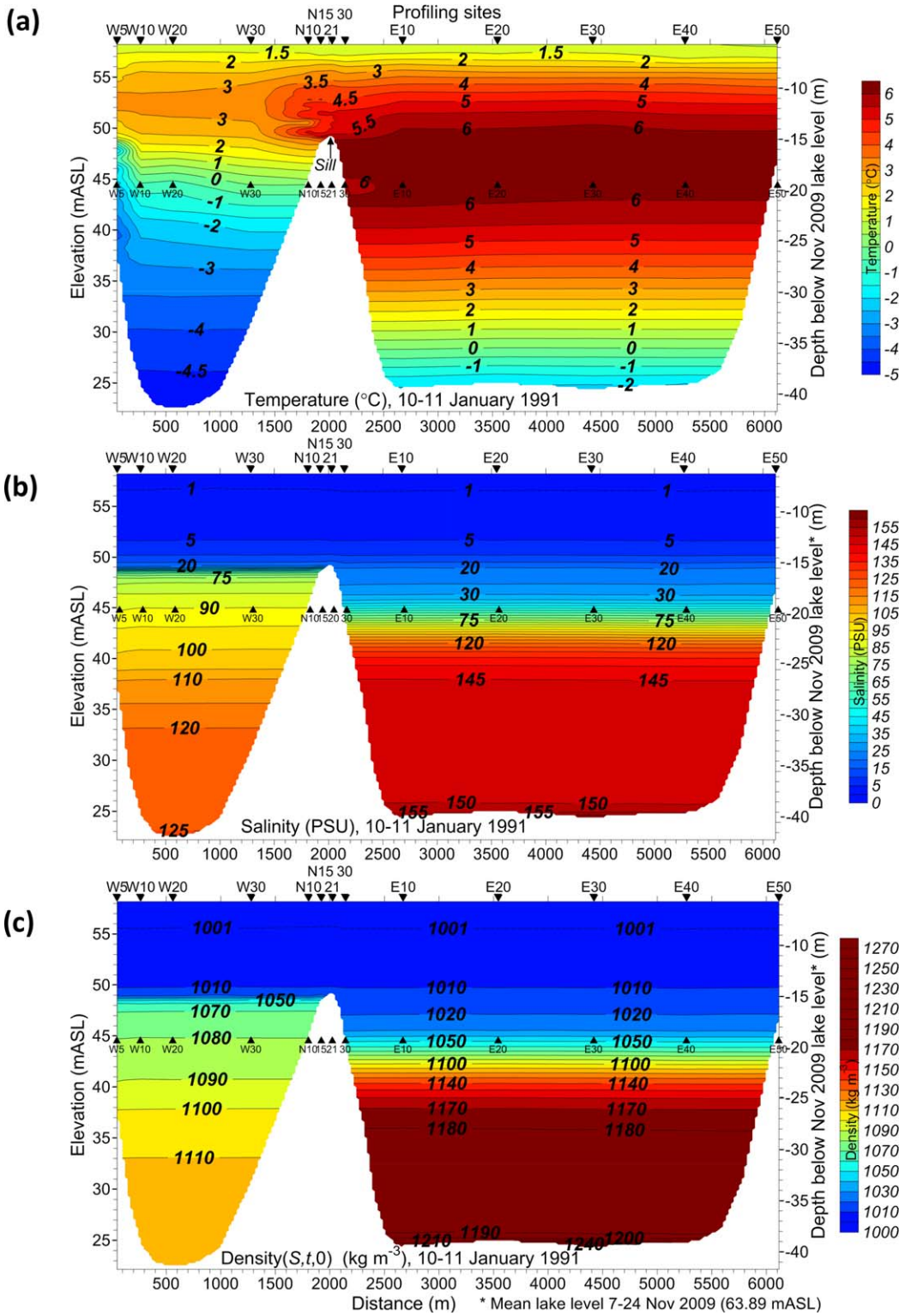

Fig. 3. Contour plots from a CTD transect made on 10 January 1991–11 January 1991 through WLB and ELB, based on profiles presented in Spigel and Priscu (1998); the locations of profiling sites are shown by black triangles at the top of each plot. Depths shown on right-hand axes are relative to mean water levels 07 November 2009–24 November 2009, 63.89 mASL. Depths below the bottom-most point of each profile have been masked, except through the narrows where data from an ENDURANCE sonar survey (unpublished data) have been used to extend the mapped region to the depth of the sill that separates ELB and WLB. CTD data between the bottom of measured profiles and the channel bed have been interpolated and extrapolated from neighboring sites. (**a**) Temperature. (**b**) Practical salinities. (**c**) Density at atmospheric pressure (a close approximation to potential density).

Results

For purposes of comparison with the 2009 results, data from a transect made on 10 January 1991 and 11 January 1991 extending from approximately 50 m off the face of the Taylor Glacier through WLB, the narrows and ELB are presented as contour plots in Fig. 3. Locations of sites in WLB and the narrows occupied during the January 1991 transect are shown in Fig. 2. Only one 1991 site in ELB is shown in the location map of Fig. 2 as *E10*. ELB extends a further 4.2 km to the east of *E10* (Figs. 1, 2), and the remaining 1991 ELB sites are indicated at the top of the contour plots in Fig. 3. Spacing between sites for the 1991 transect varied from approximately 200–700 m between profiles in WLB, 100 m in the narrows, and from 500 m to 875 m in ELB. In contrast, during the 2009 profiling horizontal resolution was approximately 25 m between profiles in the sampling grid near the glacier face; 100 m between profiles in the main body of WLB; and 50 m between profiles in the narrows (Fig. 2).

The 2009 ENDURANCE results are presented initially as contour plots in Figs. 4, 5 along two major transect lines. Figure 4, based on the 100 m grid, extends from the face of the Taylor Glacier through WLB, the narrows, and for a short distance into ELB. Figure 5, based on the 25 m grid, extends along the face of the Taylor Glacier. Figure 6 is a 3-D scatter plot of temperature based on data from all sites in the vicinity of the glacier face.

It is important to note that the CTD casts shown in Fig. 4 through the narrows separating ELB and WLB (sites D21 – NR8 in Fig. 2) were made near the centerline of the channel. Subsequent analyses of bathymetry deduced from sonar measurements indicated that this was not the deepest part of the channel. The longitudinal cross-section through the sill in the narrows as shown in Fig. 4 represents our best current estimate of the depth to the deepest part of the channel, and the dashed line above the bottom indicates the bottom limit of the CTD casts, which were stopped approximately 1 m above the bed at the cast sites. The contours shown in Fig. 4 between the dashed line and the bottom in the narrows are therefore not based on measurements at those points but rather on interpolation and extrapolation of measurements at adjacent profiling sites.

Results are presented in Fig. 7 for profiles along a transect line extending from the glacier face into WLB through the 25 m grid for sites BF34-BF30 and including sites D3 and D4 from the 100 m grid (site locations highlighted in yellow in inset of Fig. 2). Also shown are profiles measured on 11 January 1991 for sites W5, W10, and W20. W5 was the only near-glacier site occupied in 1991, while W20 is representative of the main body of WLB. Figure 7a includes both in situ temperatures and freezing-point temperatures computed from in situ salinities and pressures (*see* "Methods" section). Figure 5b shows contours of the difference between in situ and freezing-point temperatures in the water adjacent to the glacier face. Figure 7b shows profiles of density for the BF34-BF30 and W5-W20 sites. Individual profiles used to construct the contour plots in Figs. 4, 5 are shown in Fig. 8.

All plots include two axes for water depth, one as elevation above mean sea level, the other as depth below piezometric water level during the 2009 profiling period. Although depth below water surface provides a more intuitive measure, we have used elevation above sea level in order to make consistent comparisons between measurements made in 1990–1991 and November 2009. Lake level has varied considerably over this period, rising (though not at a steady rate) from 62.18 mASL on 27 January 1991, to 63.89 mASL for 07 November 2009 to 24 November 2009.

General features of the temperature-salinity-density structure

One of the most striking features of the contour plots for both the 1991 and 2009 data, as shown in Figs. 3–5, is the extreme flatness of the density and salinity contours, especially when compared with the much greater horizontal variability of the temperature contours. Density stratification is controlled almost exclusively by salinity, with temperature having a relatively minor influence. This is because of the large range and the strong vertical gradients of salinity in comparison with those of temperature, which varies over a relatively small range. The plots of density therefore closely mirror those of salinity. In contrast, temperature acts as an almost passive tracer, and can be used to help differentiate water sources and to provide information on water movements.

Comparison of Figs. 3, 4 shows strong similarity in the main features of temperature, salinity and density structure between the 1991 and 2009 longitudinal transects. The level of the halocline (the region of steepest salinity gradient) in WLB remained fixed just below the top of the sill in both years, with water adjacent to the Taylor Glacier being cooler than in the rest of WLB, and water in ELB being warmer than in WLB.

Because of the dominant influence of salinity on density in Lake Bonney, the halocline and pycnocline (region of steepest density gradient) coincide, around the depth of the 40 PSU contour for salinity and the 1040 kg m^{-3} contour for density in WLB. Profiles for individual dissolved solutes, not shown here, all exhibit a similar pattern. In the remainder of this paper, we will refer to the region of steepest salinity, density, and chemical gradients as the chemocline.

Notable in Figs. 3a, 4a, 6, 7a are cooler temperatures that extend from the glacier face, suggestive of cooler flows propagating from the glacier into WLB, and the interleaving over the sill separating WLB from ELB of warmer ELB temperatures with the cooler temperatures of WLB, suggestive of an exchange between waters of WLB and ELB above the sill.

Near-glacier temperature anomaly

The submerged face of the Taylor Glacier acts as a heat sink for WLB, and this is one reason for the cooler

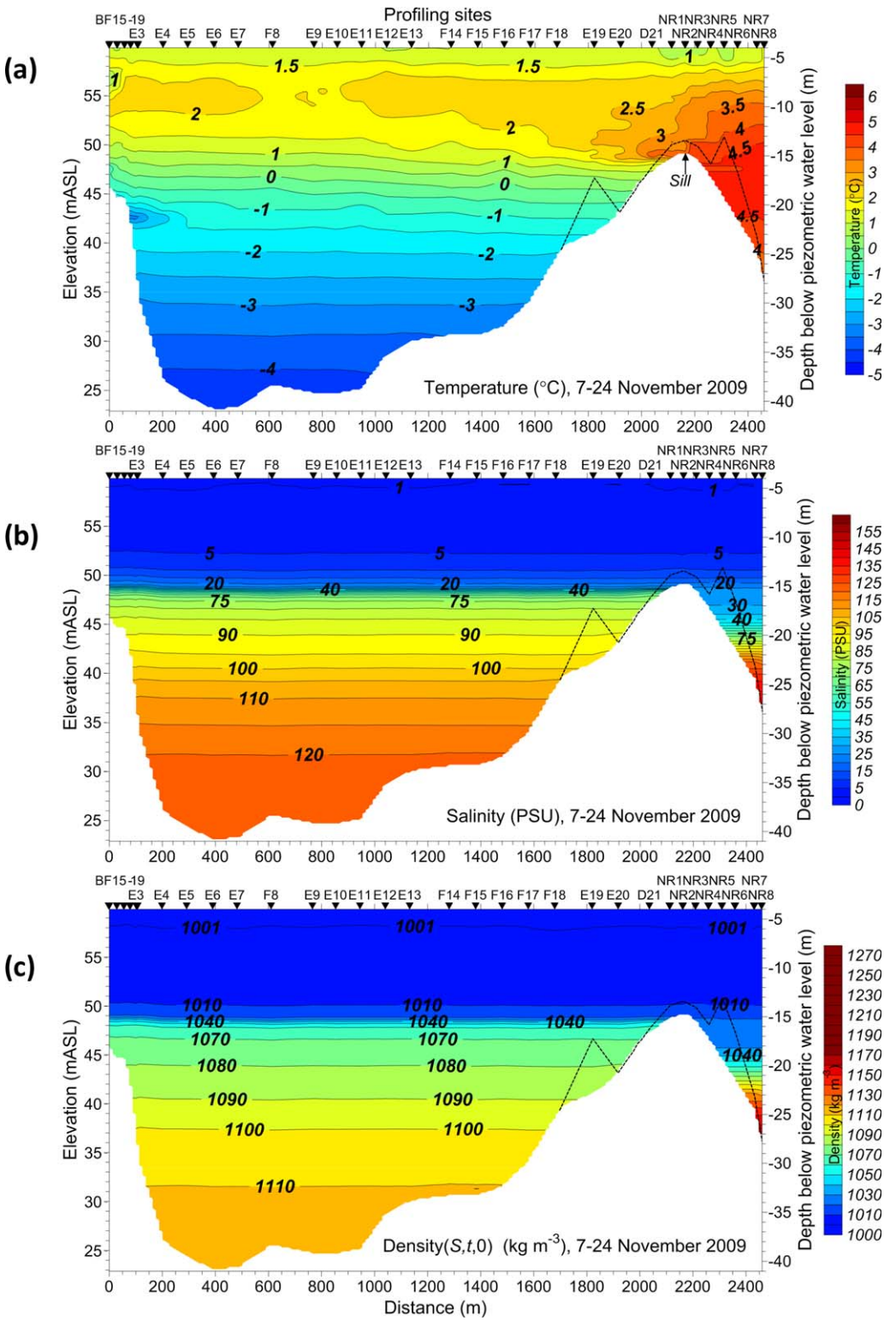

Fig. 4. Contour plots from a west-east transect in November 2009 from the front of the Taylor Glacier through WLB and narrows to the start of ELB. Locations of profiling sites, masking below depth of profiles, and extension of profile depths to sill elevation through the narrows are as described in the caption for Fig. 3. The dashed black line above the lake bottom through the narrows indicates the actual depth of CTD profiles; contours in the region between the dashed line and the estimated depth of the lake bed have been extended by extrapolation from neighboring sites. (**a**) Temperature. (**b**) Practical salinity. (**c**) Density at atmospheric pressure.

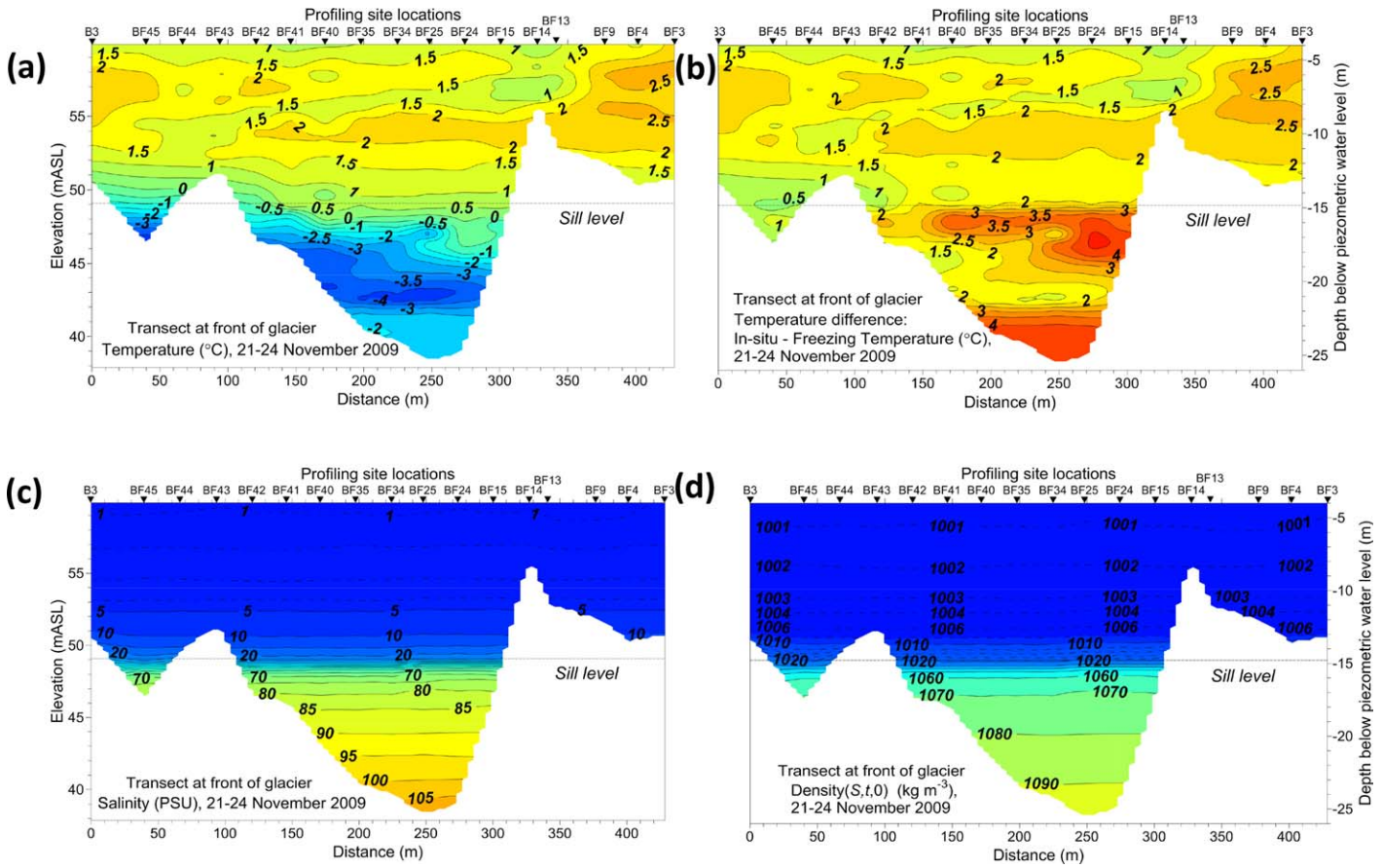

Fig. 5. Contour plots of a south-north transect across the front of the Taylor Glacier from selected ENDURANCE sites in the sampling grid shown in the inset of Fig. 2 All depths below the bottom-most point in each profile have been masked in the contour plots. (**a**) Temperature contours. (**b**) Temperature difference in water at the glacier front between the melting point temperature (computed from in-situ salinity and pressure) minus the in-situ temperature. (**c**) Practical salinity. (**d**) Density at atmospheric pressure. Color scales of contours for temperature, salinity and density are the same as those in Fig. 3 and Fig. 4.

temperatures of WLB overall compared to ELB (Figs. 3a, 4a), as well as for the cooler temperatures near the glacier face in WLB. Figure 6 provides a striking illustration of the extent of these colder temperatures, which we refer to as "the temperature anomaly" because of the marked contrast between differences in temperature compared to the horizontal uniformity of salt and density that characterize stratification in the lake. Figure 7a is typical of temperatures measured along transect lines extending from the glacier face into the main body of WLB, with colder temperatures in 2009 extending to a depth of about 23 m. Visual images recorded from the ENDURANCE (not shown) indicated that this depth marked a boundary between exposed glacier ice and bottom sediments.

The 1991 profiles from sites W5, W10, and W20 also show a temperature anomaly, but one that extends to a greater depth than in 2009 ($\sim$ 26 m). This difference is likely due to changes in the configuration of the glacier front between 1991 and 2009. Fountain et al. (2004; Table 1, p. 559) estimated that the terminus of the Taylor Glacier advanced approximately 100 ($\pm$ 11) m over 20 yr between 1976 and 1996. Unpublished photographs (Fountain pers. comm.) indicate that the advanced part of the glacier calved into the lake sometime between 1998 and 2006, restoring the position of the terminus to its 1976 position. Calving therefore occurred at some time between the measurements made in 1991 and 2009, and could have altered the depth of the temperature anomaly at the glacier face over time.

The temperature profiles shown in Fig. 7a are indicative of cold intrusions at different scales propagating from below the glacier face into WLB. The larger-scale intrusions, present in both 1990–1991 and 2008–2009 measurements, are likely associated with cold, saline inflows derived from the subglacial brines described by Mikucki et al. (2015) and Badgeley et al. (2017), who propose that they drain from the base of the submerged glacier terminus into WLB. They are not apparent in the salinity profiles, but this would be expected if they are weak flows intruding at their level of neutral buoyancy.

Finer-scale layering can be seen in the 1990–1991 temperature profile at W5, most pronounced between 44 mASL and

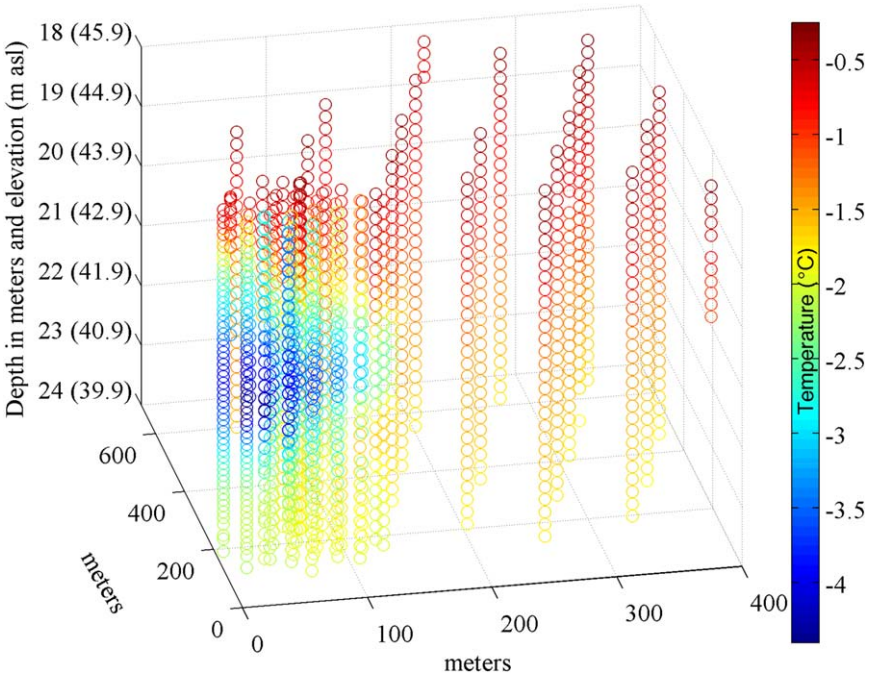

Fig. 6. Three-dimensional temperature plot illustrating the extent of the cold-water temperature anomaly in front of the glacier based on 2009 measurements. Horizontal axes give distance east and north, with origin as shown by E,N axes in inset of Fig. 2. The plot utilizes most sites shown in the inset of Fig. 2 as well as some points from the 100 m grid. Note the difference in color-scale from that used in the contour plots.

46 mASL. Corresponding layering is also present in W5 profiles of salinity and density (Fig. 7b), although not easily seen at the scale of this figure. In contrast, the 2009 measurements were made at a lower frequency and higher drop speed, with an average distance between sampling points of 20 cm, and would not have been able to resolve the finer-scale layers if they had been present. We believe that the layering is derived from melting of the exposed glacier face into the salinity gradient below the chemocline, described in more detail in the "Discussion" section. Salinity stratification is largely absent above the chemocline, and the layering is not present there, although melting of the glacier face must also be occurring because of the >0°C water temperatures.

Figure 9 shows a segment of the earlier profiles in more detail, including all four sets of casts made during the 1990–1991 season at the W5, W10, and W20 sites, from 24 November 1990 to 12 January 1991. The layers appear as asymmetrical, oscillatory-like features in the profiles of temperature, salinity, and density. The consistency over the 7-week time span in the elevations and amplitudes of the oscillations is striking; as expected, the temperatures are more variable than the salinities. In all plots the cooler temperatures coincide with lower salinities, and warmer temperatures with higher salinities at the W5 site, suggestive of intrusion layers derived from melting at the glacier face (discussed in more detail below). The oscillations have largely decayed at site W10, except for the 29 November 1990 profile, where attenuated oscillations are visible, but out of phase with those at W5; this would be the case if the layers represented intrusions that were propagating along a slightly sloping direction instead of strictly horizontally. The sampled data points are plotted in Fig. 9, showing the resolution of these features by the CTD.

In the "Discussion" section, we explain why we believe these oscillations are a signature of intrusions in which double diffusion, occurs. As pointed out by Spigel and Priscu (1998) in relation to profiles measured in 1990–1991, the vertical variation of temperature of maximum density indicates that in WLB the temperature profile is stable over almost the entire water column, ruling out the possibility of double diffusion in the interior of the basin; this is also true for the 2009 profiles (Fig. 7a). However, in the finer-scale layering just described, layers of warmer, more saline water alternate with cooler, fresher waters, providing evidence for the occurrence double diffusion near the glacier face in the oscillatory features of Fig. 9.

Discussion

A conceptual model

A conceptual model that illustrates inflow, melt and circulation processes associated with the results presented above is shown in Fig. 10. The model shows circulations in the upper, fresher waters above the chemocline, transports of water and salt below the chemocline, and interactions between ELB and WLB above the sill in the narrows. The

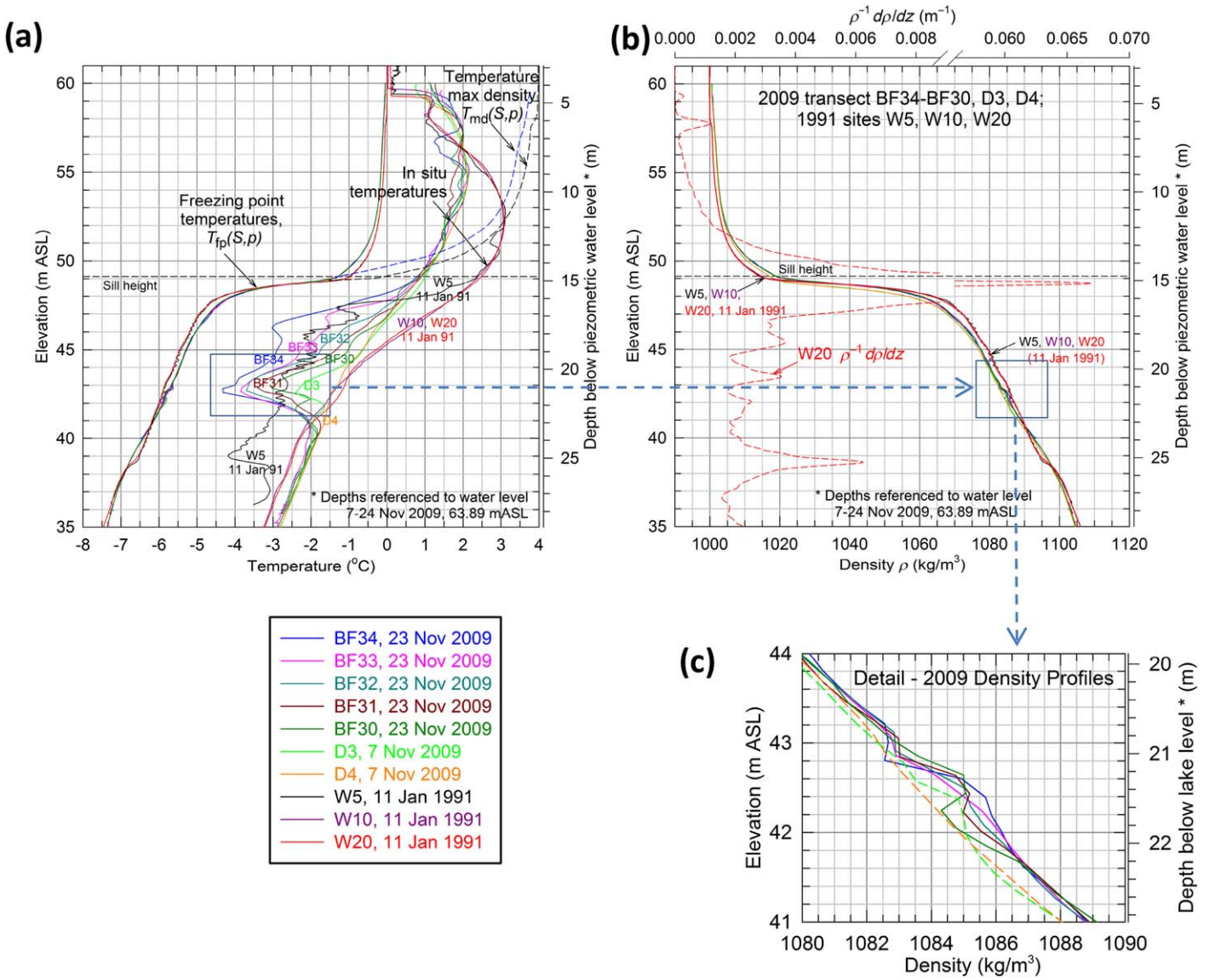

Fig. 7. (**a**) Temperatures and (**b**) densities, at BF34-BF30, D3, D4 (November 2009), and W5–W20 (January 1991), with far-field (W20) density gradient used for analysis of W5 intrusion thicknesses; plots include and freezing-point temperatures (**a**) and densities (**b**) calculated from salinity profiles at W5 and W20. (**c**) Detail (region outlined by box in (**a**) and (**b**)) from 2009 density profiles showing possible overturning and instability in cold intrusion. All depths are referenced to average lake level between 07 November 2009 and 24 November 2009 (63.89 mASL).

model provides a framework for discussion of these processes below. We will provide quantitative estimates for melt-related processes (darker blue arrows above the chemocline, green arrows below the chemocline), but for some of the processes (exchange above the sill, cold saline inflows below the chemocline) we are unable to make quantitative analyses.

Cold, saline sub-chemocline inflows

Mikucki et al. (2015) have presented analysis and imagery of the resistivity field beneath Taylor Valley, as measured by airborne electromagnetic surveys. They interpreted the results as an indication that liquid with high solute content exists at temperatures well below 0°C as sub-glacial brines, and that some of these inferred brines emanate from below Taylor Glacier into Lake Bonney. Since then, Badgeley et al. (2017) have used radio echo sounding and hydraulic-potential modeling to map the flow of these brines under the base of the Taylor Glacier terminus, and have proposed that some of the sub-glacial brines drain into WLB, although they have not provided estimates for the volumes of such flows. They have also mapped flow pathways within the glacier terminus itself, showing hydraulic connectivity between the cold basal brines and a supra-glacial brine outflow known as Blood Falls (because of its red color caused by high

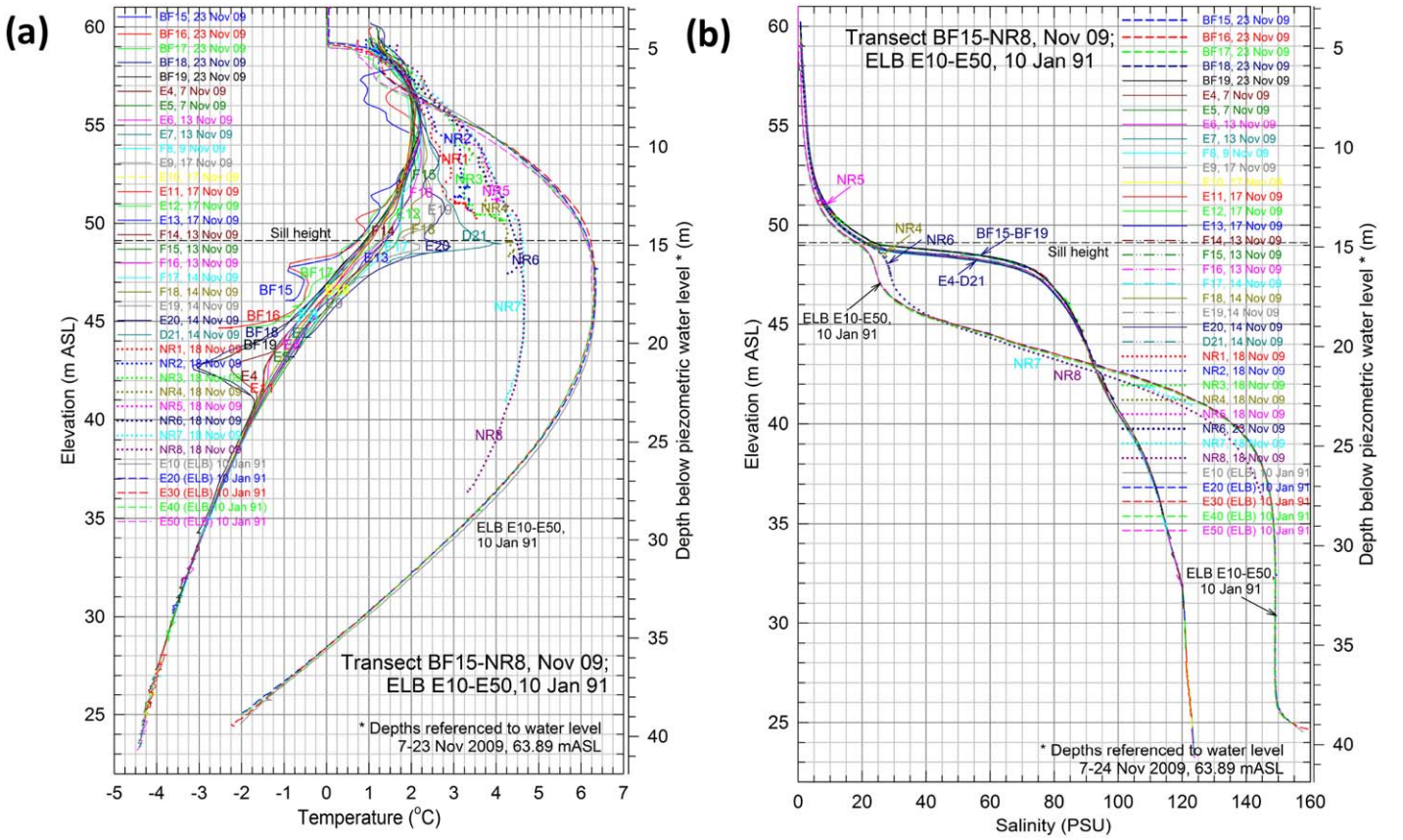

Fig. 8. (**a**) Temperature, (**b**) salinity – main west-east transect from glacier through WLB, narrows and start of ELB, BF15-NR8; with 10 January 1991 ELB profiles E10–E50. Depth scale is referenced to mean lake level (63.89 mASL) over the period of measurements 07 November 2009–24 November 2009.

concentrations of iron), that exits the glacier above ground at the glacier terminus (Mikucki et al. 2004, 2009; Mikucki and Priscu 2007).

These processes are identified in Fig. 10 by bright and dark red arrows. We believe that our results reflect the inflow of these brines, either directly as drainage from the basal glacier system, as described by Badgely et al. (2017), or as a density current that originates at Blood Falls (e.g., Mikucki et al. 2004, their Fig. 2, showing an iron-rich lens below the WLB chemocline near 25 m). The clearest illustrations linking such cold, saline inflows to possible intrusions in WLB come from transects extending from the glacier face and through the sites of the 25 m grid into WLB, one of which (BF34-BF30, D3, D4; *see* Fig. 2, where these sites are highlighted in yellow in the inset) is shown in Fig. 7. The 2009 temperature profiles in Fig. 7a have two local minima below the chemocline, the coldest at a depth of 21 m, with the anomaly in temperature decreasing gradually with distance from the glacier face. The shapes of the profiles are suggestive of intrusions propagating from the glacier terminus into WLB, gradually coming to thermal equilibrium and mixing with their surroundings. Although adjustment appears nearly complete by site D4 in Fig. 7a, a distance of approximately 200 m from the glacier face, closer examination of profiles measured on the full transect through WLB (Fig. 8) indicates that colder temperatures persist as far as site F8 at a distance of approximately 600 m from the glacier face, with complete adjustment not evident until site E9 at a distance of approximately 700 m. Profiles measured during December 2008 (not shown, but similar in form to those shown in Fig. 8) indicated that the temperature anomaly occupied a smaller area, with colder temperatures at D7 (~ 500 m) and complete adjustment by D8 (~ 600 m). Density profiles for the near-glacier 25 m grid in 2009 (Fig. 7b, and detail in Fig. 7c) show evidence of possible overturn associated with the intrusion at 21 m as it evolves from a slight distortion in the density profile at B34 closest to the glacier, to an unstable configuration at B30, and back to a stable profile at D4. Other transects, not shown (BF 24-BF20; BF25-BF29; BF35-BF39), all exhibit similar features, including possible instability around 21 m.

Evidence for the hypothesized sub-chemocline inflows is not readily apparent in the salinity contour plots, as would be expected if the inflows enter WLB from under or within

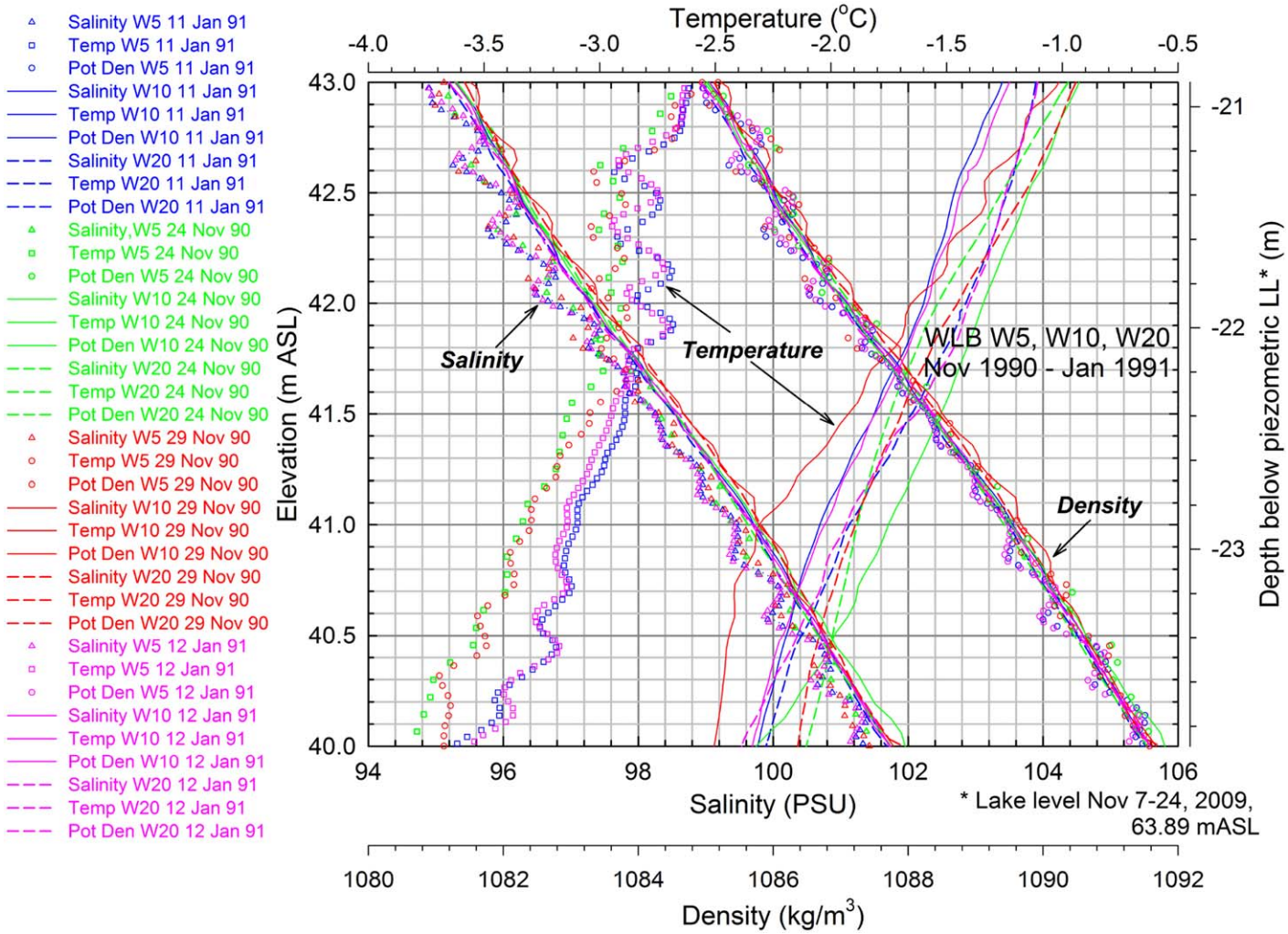

Fig. 9. Profile segment detail for CTD casts in WLB made on 24 November 1990, 29 November 1990, 11 January 1991, and 12 January 1991 at sites W5, W10, and W20. Sample points are plotted for the W5 (near-glacier) site, showing the resolution of the meltwater intrusions. Evidence of intrusions persisting to site W10 can also be seen in the profiles for 29 November 1990, with oscillation out of phase with W5 profiles, consistent with a slight upward slope of the intrusions.

Taylor Glacier and then flow along the glacier face until they reach their level of neutral density in the lake near the glacier face. These inflows would then flow out into the lake at that depth carrying the same salinity as the surrounding water, but a different temperature. The temperature anomaly would gradually disappear with distance along the intrusion due to mixing and heat transfer with the surrounding ambient lake water. At the same time, MacIntyre et al. (2006) have shown that thin-layer formation in regions of strong stratification comparable to those below the WLB chemocline can act to increase intrusion lengths.

Melting at the submerged glacier face

Melting processes at the submerged glacier face are identified in Fig. 10 by darker blue arrows in the waters above the chemocline, and by the pairs of green arrows associated with layering and finer-scale intrusions below the chemocline; melting processes are quite different above and below the chemocline, and need to be analyzed by different methods.

As noted above in "Near-glacier temperature anomaly" section Fountain et al. (2004, Table 1, p. 559) estimated that the terminus of the Taylor Glacier advanced approximately 100 (± 11) m over 20 yr between 1976 and 1996. Although the advance and subsequent calving and melting probably did not occur uniformly over time, the observations can be used to give an order of magnitude estimate of 5 m yr^{-1} for a melt rate. More recently, Pettit et al. (2014) have provided detailed analysis of the flow of the Taylor Glacier terminus; their Fig. 3 shows estimates for varying flow speeds at different locations on the glacier terminus, with a value of 5.3 m yr^{-1} where the terminus enters WLB. These estimates provide some context for melt estimates calculated below.

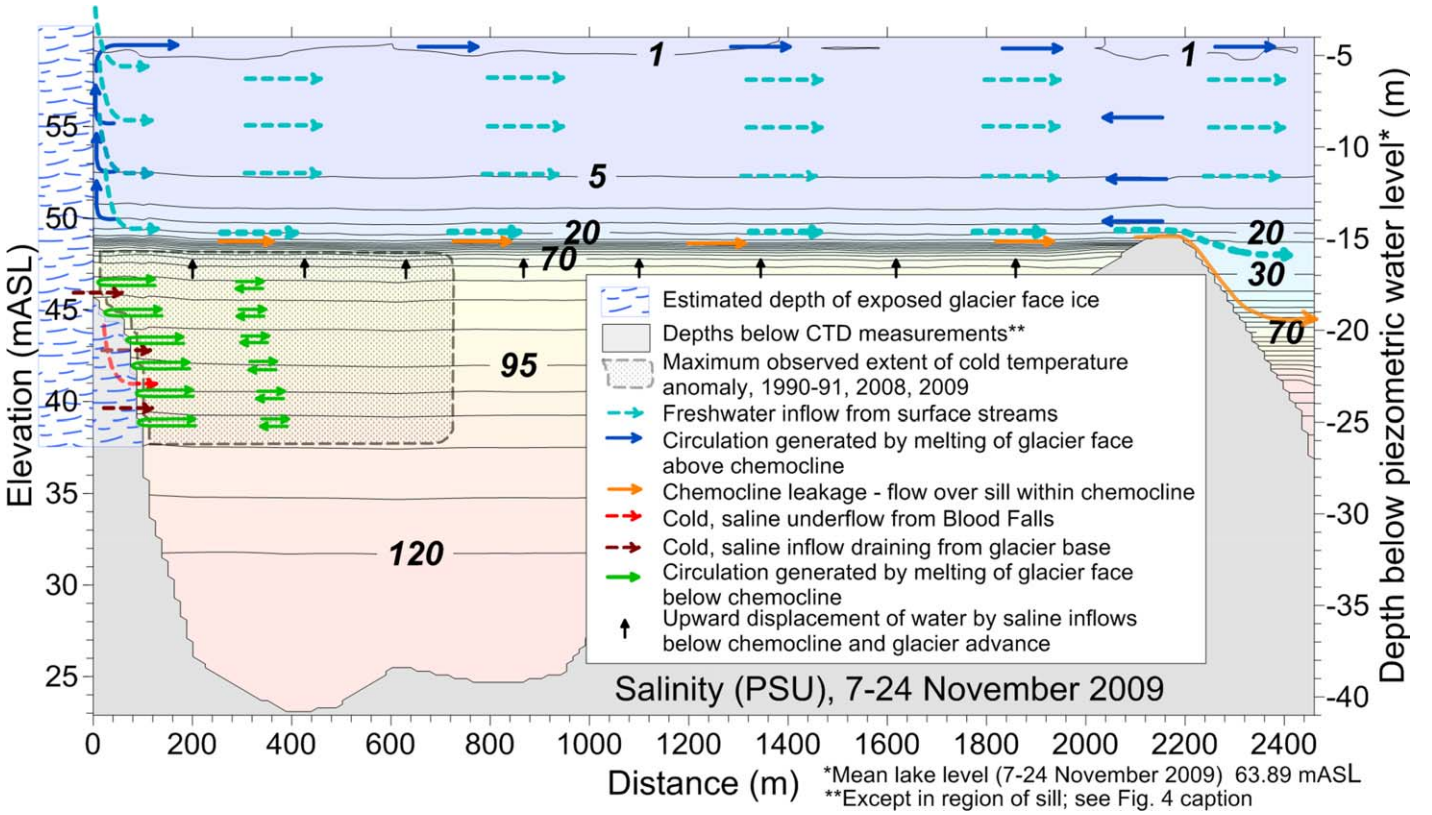

Fig. 10. Conceptual sketch summarizing inflow, melt and circulation processes.

Thermal energy for melting of the submerged glacier face is supplied by the heat stored in the water column, and to a minor extent by solar radiation that penetrates the lake's ice cover. To estimate of the relative contribution from solar radiation we used measurements from the Lake Bonney LTER Meteorological Station (http://www.mcmlter.org/content/lake-bonney-meteorological-station-measurements) to obtain a typical value for the peak radiation months November–February for incoming phothosynthetically active radiation (PAR) of 600 μmol m^{-2} s^{-1} (maximum 15-min values can be around 1200 μmol m^{-2} s^{-1}). We assumed that 2.5% of incoming radiation penetrates the ice (Lizotte and Priscu 1992 specify a range from 1% to 5%), use a conversion of quanta flux to energy flux of 4.6 μmol quanta/joule (Kirk 1994) to obtain 3.26 W m^{-2} below the ice (peak values 6.52 W m^{-2}), and assume an exponential decay of the solar flux through the water column with an attenuation coefficient of 0.15 m^{-1} (Lizotte and Priscu 1992 specify a range of 0.1–0.2 m^{-1}). If we neglect any directionality of the underwater radiation, assuming it is mostly diffuse, then the available energy decays from 3.26 W m^{-2} at 4 m to 0.012 W m^{-2} at 26 m, which we assume to be the extent of the exposed ice face (assuming a directionality for the radiation would reduce these values). The energy flux can be converted to a melt rate $\dot{m}(z) = I(z)/(\rho_{\text{ice}}\, L)$, where $\dot{m}(z)$ is the melt rate, $I(z)$ is the underwater irradiance, ρ_{ice} is the density of ice (assume 916.8 kg m^{-3}) and L is latent heat of fusion (assume 334 kJ kg^{-1}), giving melt rate values of 2.8 cm month^{-1} at 4 m depth to 1 mm month^{-1} at 26 m. Melt rate can be converted to volumes of freshwater by integration over the area of exposed ice. To do this we use the provisional bathymetry estimated from the ENDURANCE sonar data by Doran (unpubl. data) to approximate the exposed ice face as a trapezoid with top width of 525 m at 4 m depth to 96.8 m at 26 m, giving volumetric melt rate values of 74 m^3 month^{-1} for an incoming energy flux or power received of 8620 W and an average flux per unit area of 1.3 W m^{-2}. To make a rough comparison of the estimated melt from solar radiation with the annual values of approximately 5 m yr^{-1} based on glacier advance from Fountain et al. (2004) and Pettit et al. (2014), we can assume that the solar melt rates above are characteristic of the 4 months November–February, implying melt rates of 11 cm yr^{-1} at 4 m to 4 mm yr^{-1} at 26 m. Assuming a longer time span for the duration of solar melt would increase these values slightly, but would not alter the basic conclusion that melting by solar radiation incident on the submerged glacier face provides a very minor contribution to total likely annual melting (cf. estimate of 5 m yr^{-1} mentioned in the previous paragraph).

Considering next latent heat transfer from water in WLB, Figs. 5b, 7a show that in situ temperatures exceed freezing-point temperatures over the entire depth of WLB, due to high salinities below the chemocline and >0°C temperatures

above the chemocline. Consequently melting of the submerged glacier must be occurring at all depths; however, two different analyses are needed to estimate melt rates. For depths above the chemocline, where salinity stratification is largely absent and the ice is melting into nearly freshwater at relatively uniform temperature, we used Bendell and Gebhart's (1976) theoretical and laboratory study. For depths below the chemocline, where ice is melting into a salinity gradient, we used Huppert and Turner's (1978, 1980) and Huppert and Josberger's (1980) results from their theoretical and laboratory studies and the related oceanic work of Jacobs et al. (1981), Stephenson et al. (2011) and others cited below. Josberger and Martin (1981) have presented results of a thorough study of an ice wall melting in water of uniform salinity within the oceanic range. While their numerical results are not directly applicable to the Taylor Glacier, their descriptions provide insight into the physical processes occurring in the meltwater boundary layer next to the ice.

All of the above studies indicate that melting generates a meltwater boundary layer next to the ice face in which the temperature and salinity vary from those at the ice–water interface at the ice surface (T_w, S_w) to those in the ambient water in the far field (T_∞, S_∞). For the purposes of our calculations, we will assume that temperatures and salinities at site W20 are representative of the far field. The magnitudes of T_w, S_w are less certain. All studies agree that T_w and S_w must lie on the freezing-point depression curve, f_{fp}, that relates freezing point temperature T_{fp} to salinity S and pressure p, although the effect of pressure is minor at the depths considered for WLB, $T_{fp} = f_{fp}(S,p) \approx f_{fp}(S)$ (Millero and Leung 1976; Fofonoff and Millard 1983; Lide 2005). For the case of freshwater in both the far field and at the ice face, which we assume to be a realistic approximation for the Taylor Glacier above the chemocline, $T_{fp} = T_w = 0$°C at atmospheric pressures. For the case of $S_\infty > 0$, Huppert and Turner (1980) and Huppert and Josberger (1980) suggest that S_w will be less than S_∞, but that as S_∞ increases T_w will tend to approach $f_{fp}(S_\infty)$, the freezing point temperature evaluated at the far-field salinity. These are the freezing point temperatures plotted in Fig. 7a and are used to calculate the differences from freezing point in Fig. 5b. Also plotted in Fig. 7a are temperatures at which maximum water density would occur for the salinities and pressures in the water near the glacier face, $T_{md}(S,p)$, as measured at W5 in January 1991 and at BF34 in November 2009 (Caldwell 1978). Note that water temperatures in WLB are below T_{md} above the chemocline, so that cooling by loss of heat transferred to the glacier for melting will make the cooled water less dense and its increased buoyancy will cause it to rise within the meltwater boundary layer. Below the chemocline, where a maximum density anomaly does not exist for liquid water at the high salinities in WLB, the opposite is the case, and cooling results in density increase. However, salinity is also reduced due to mixing with fresh meltwater in the meltwater boundary layer, resulting in a density decrease that offsets the density increase from cooling. The control of buoyancy by salinity is evident in the profiles in Figs. 5, 9, where salinity dominates the density field.

Consider first melting above the chemocline between depths in WLB where salinity can be neglected (4–14 m) and $T_w \approx 0$°C. Recent data from a sensor moored at the center of WLB at 11 m (Obryk et al. 2016) indicates that T_∞ can be approximated by a sinusoidal variation with a mean of 1.56°C and amplitude 0.125°C (*see* also Fig. 4). Water in the meltwater boundary layer will be fresh and at temperatures between 0°C and 1.56°C and, as noted above, will rise along the glacier face. The boundary layer will continue to grow until it reaches the bottom of the ice cover, where it will be turned to flow horizontally into WLB. Ambient water entrained into the rising boundary layer will be replaced by a flow in WLB toward the glacier face; this circulation is depicted by the darker blue arrows above the chemocline in Fig. 10 and its influence may extend throughout WLB and to the narrows (*see* also, e.g., Schneider 1981). Heat transfer Q to the ice face is estimated from Bendell and Gebhart (1976) as $Q = \dot{m}L/(BH) = \mathrm{Nu_H}\ k\ (T_\infty - T_w)/H$, where Q is heat flux per unit area, $\dot{m}$ is the melt rate (mass of ice per unit time), L is latent heat of fusion, B and H are width and height of the melting vertical ice face, $\mathrm{Nu_H}$ is the experimentally determined Nusselt number (dimensionless heat flux), k is thermal conductivity, and we have omitted the factor of 2 in Bendell and Gebhart's (1976) Eq. 2 that applies to the two sides of the melting ice block in their experiments. From Bendell and Gebhart's (1976, Fig. 4 and Table 1), we estimate $\mathrm{Nu_{0.303m}} = 70$, where 0.303 m is the height of the ice face in their experiment. Bendell and Gebhart (1976, Table 1) specify that to apply this to ice faces of height H it should be multiplied by $(H/0.303)^{3/4}$, giving $\mathrm{Nu_H} = 964$ for $H = 10$ m, considering the Taylor Glacier from 14 m to 4 m (and assuming the upscaling to 10 m is valid). This is an average Nusselt number, i.e., it represents an integral over a rectangular ice area, but we will use it to estimate the average heat flux over the trapezoidal area of Taylor Glacier face (top width 525 m at 4 m, as above, and bottom width 430 m at 10 m). Taking thermal conductivity $k = 0.556$ W m^{-1} K^{-1} (Ramires et al. 1995), gives $Q = 83.4$ W m^{-2} and a corresponding melt rate $Q/(\rho_{ice}\ L) = 8.6$ m yr^{-1} (or a mean monthly rate of 0.72 m month^{-1}). This is of similar magnitude, although somewhat larger, than the 5 m yr^{-1} estimated from glacier advance.

Below the chemocline melting occurs into a salinity gradient, and the fresher meltwater would not flow vertically upward along the glacier face for any considerable distance. Water in the meltwater boundary layer encounters progressively less salty, and hence less dense, water in its surroundings as it rises through the salinity gradient, until it reaches its level of neutral buoyancy. It then propagates as a series of nearly horizontal intrusions into the surrounding ambient

water, as explained by Huppert and Turner (1978, 1980) and Huppert and Josberger (1980) in relation to their laboratory experiments with ice blocks melting into a salinity gradient. Their results showed that the presence of a horizontal temperature gradient generated by melting, in combination with a vertical salinity gradient in the ambient water, altered the boundary layer a small distance from the ice and produced a regular series of slightly tilted convecting layers which grew out into the surrounding water. "Along the top of the layers there is an inflow of environmental fluid, which is directly mixed with the melt water only near the ice. In this way, a considerable portion of melt water can be fed into the environment close to the level at which it is produced and very little, if any, rises to the surface." (Huppert and Turner 1978). This process was further documented in subsequent laboratory, field and numerical studies by Jacobs et al. (1981) for the Erebus Glacier tongue in the Ross Sea; Oshima et al. (1994) for icebergs trapped by fast ice in Lützow-Holm Bay, Antarctica; Stephenson et al. (2011) for a large free-floating iceberg in the Weddell Sea; and Gayen et al. (2015) in numerical computer simulations. We hypothesize that the layering observed in the 1990–1991 data (Fig. 9) is caused by intrusions propagating from the melting glacier face, as illustrated by the pairs of green arrows below the chemocline in Fig. 10, and that the wavelengths of the oscillations are measures of the thickness of the intrusions. However, before presenting further analysis in support of this hypothesis we make two observations.

First, these types of intrusions have also been associated with double diffusive convection, generated by heating or cooling at sidewalls in an ambient fluid that contains competing gradients, in terms of static stability, of temperature and salinity (or of gradients of concentrations of two solutes such as sugar and salt); see, e.g., Turner (1978), Huppert and Turner (1981), Jeevaraj and Imberger (1991) and Schladow et al. (1992). We point out that the background or ambient stratification in WLB below the chemocline is composed of gradients that are stable for both temperature and salinity, hence not susceptible to onset of double-diffusive instability in the absence of some external forcing from boundaries. However, once the intrusions are generated by melting, they do possess double-diffusive properties within the alternating layers of inflowing warmer, more saline ambient water and outflowing cooler, fresher water. Huppert and Turner (1981, p. 306) point out that "the mechanism of introducing cold melt water laterally allowed double diffusive steps to occur even in the presence of profiles of temperature which decreased and of salinity which increased with depth. These distributions by themselves are not subject to double-diffusive instabilities…," while Malki-Epshtein et al. (2004), have presented a theoretical and laboratory study that considers double-diffusive aspects of intrusions propagating into a salinity gradient from a vertical cooled wall, with no melting or far-field temperature gradients.

Second, while we are confident that shape of the temperature and salinity profiles have been satisfactorily resolved by our measurements, and are not artefacts of the sampling procedure or instrument malfunction, we are puzzled by the pronounced oscillatory shape of the profiles that, while not symmetrical about their local minim and maxima, are not statically stable in the shorter segments where warmer, saltier inflowing water overlies cooler fresher outflowing water. In contrast, the profiles presented by Jacobs et al. (1981) exhibit the staircase pattern characteristic of double diffusive layers. The experimental results of Huppert and Turner (1980) and Malki-Epshtein et al. (2004) are not presented as profiles, but in terms of shadowgraphs, dye traces and other flow visualization techniques, so comparison with our profiles is not possible. An experimental profile of salinity measured near the sidewall by Schladow et al. (1992) does exhibit an exactly similar shape to those measured at W5 (Fig. 9), while profiles measured farther from the wall are stable. Numerical calculations presented by Schladow et al. (1992) indicate that overturning is occurring in these layers close to the wall, and that with distance from the wall a stable configuration evolves. The very close proximity of site W5 to the glacier face seems to be the most likely explanation for the patterns observed in Fig. 9. In the only profile for which the intrusions can still be detected at site W10 (29 November 1990), the density profile is completely stable.

To support our hypothesis that the layering in Fig. 9 is a manifestation of the intrusion processes described above, we first show that the layer thicknesses of our data are consistent with values presented in the literature. Based on the results of their laboratory experiments, a simple scaling relation for the layer thicknesses was proposed by Huppert and Turner (1980) and Huppert and Josberger (1980), $h\ (d\rho/dz)/[\rho(S_\infty,T_{fp}) - \rho(S_\infty,T_\infty)] = 0.65$, where h is the layer thickness (m), S_∞ and T_∞ are far-field salinity and temperature characterizing the water into which the ice is melting, T_{fp} is the freezing-point temperature corresponding to salinity S_∞, $\rho(S_\infty,T_{fp})$ is density (kg m^{-3}) corresponding to salinity S_∞ and temperature T_{fp}, $\rho(S_\infty,T_\infty)$ is ambient far-field density (kg m^{-3}) corresponding to salinity S_∞ and temperature T_∞, and $d\rho/dz$ is the ambient far-field density gradient (kg m^{-4}). The constant 0.65 was based on fitting to experimental data. We measured 29 thicknesses from the W5 data shown in Fig. 9 for 11 January 1991, between depths 16–25 m. Thicknesses ranged from 10 cm to 34 cm, with mean thickness of 22 cm (median 23 cm, standard deviation 6.8 cm). Non-dimensional intrusion thicknesses $h\ (d\rho/dz)/[\rho(S_\infty,T_{fp}) - \rho(S_\infty,T_\infty)]$ ranged from 0.52 to 0.87 with mean (and median) 0.69 and standard deviation 0.086. We used in situ values of S_∞ in our calculations; using the average value of S_∞, as was done by Huppert and Turner (1980) and Huppert and Josberger (1980), gave the same value of 0.69 for the mean thickness but a slightly smaller standard deviation, 0.085. Given the uncertainties involved in scaling the thicknesses from the graph, we think

that the agreement with Huppert and Turner's (1980) and Huppert and Josberger's (1980) value of 0.65 is reasonable.

The hypothesis that the layering presented in Fig. 9 is due to meltwater processes is further supported by the fact that the salinity profiles in the far field at W20 are tangent to the peaks of the salinity profiles at W5, consistent with identifying the salinity peaks with inflowing warmer, saltier ambient water and the minima with outward flowing fresher, cooler water that has been diluted by melt from the glacier face. It is also of interest that the far-field density profiles appear to pass through the means of the W5 profile. Integration of the density profiles for 11 January 1991 over the depth from 16.5 m to 26 m depth, the range over which the intrusions were observed, incorporating basin bathymetry, indicated that mass was conserved to within 0.03% between W5 and W20.

We are not aware of any methods for calculating heat transfer and melt rates directly for the thermohaline intrusions below the chemocline. However, using methods employed by Jacobs et al. (1981) and Stephenson et al. (2011), we can relate the salinity deficit in the W5 profiles to possible melt rates by calculating the amount of fresh water that would be required to reduce the salinities in the intrusions from those in the far field, and by making some assumptions about the extent of WLB affected by melt-induced circulations. These are basically salt balance calculations, and we have converted W5 and W20 salinities to total dissolved solids (TDS) concentrations before carrying out the calculations. For salinity $S < 60$ PSU, values of salinities as PSU provide a good approximation to TDS as kg salt m^{-3} of solution; for $S \geq 60$ PSU, S underestimates TDS and TDS was calculated as $TDS = 0.5219 + 0.8357\ S + 0.002636\ S^2$, from a regression ($r^2 = 0.998$) based on ion concentration data for WLB presented in Spigel and Priscu (1996). Integration from 16.5 m to 26 m depth indicated a salt deficit of 4.48 kg salt in the 9.5 m deep by 1 m^2 water column for W5 compared with W20. For a mean TDS = 104 kg salt m^{-3} at W20 over this depth, this implies a necessary replacement volume of 0.0429 m^3 freshwater with (TDS = 0) over the 9.5 m by 1 m^2 water column. If we assume an extent of influence on an annual basis corresponding to the approximate horizontal area over which the temperature anomaly was observed, from 1.3×10^5 m^2 in 2008 to 2.7×10^5 m^2 in 2009 (similar to the approach used by Jacobs et al. 1981), and use the trapezoidal approximation for the shape of the glacier face exposed to melting, we calculate melt rates of between 3.4 m yr^{-1} (2008) and 7.0 m yr^{-1} (2009), corresponding to the volumes of freshwater required from melt to account for the salt deficit calculated above.

It is difficult to relate these results to long-term projections for the evolution of salinity structure in WLB, not only because of the approximations, uncertainties and assumptions involved, but also because of our lack of knowledge about the magnitude and concentrations of sub-glacial brine inflows to WLB and of chemocline leakage over the sill from WLB to ELB. Although difficult to see on the scale of the Figs. 7b, 8b, profile data indicate that salinity decreased slightly below the chemocline over the 19 yr from November 1990 to November 2009. Integration of TDS over the entire WLB basin below sill level (49.1 m ASL, as determined from a dive survey by Peter Doran in December 2016) to elevation 24.00 m ASL (depth 39.89 m, total volume 10.7×10^6 m^3) gives a total decrease in salt of 33.3×10^6 kg of salt over 19 yr, representing 2.9% of the total basin salt content in that depth range. This can be expressed as an annual dilution rate or salinity deficit over the 19 yr of 1.75×10^6 kg salt yr^{-1}. In this form, the observed decrease in salt content can be compared to the salt deficits corresponding to the melt rates estimated in the preceding paragraph of 0.583×10^6 kg salt/year to 1.21×10^6 kg salt/year for the 9.5 m water column and areas 1.3×10^5 m^2 (2008) to 2.7×10^5 m^2 (2009). The corresponding melt from the exposed glacier face, based on the assumed area of the glacier face and a simple salt balance of the entire WLB basin below the sill, is 8.0 m yr^{-1}, the same as the estimated melt from the glacier face above the chemocline. This is somewhat larger than the values of 3.4–7.0 m yr^{-1} calculated for the intrusions and 5 m yr^{-1} estimated from glacier advance, although all of these estimates are of similar magnitude. Within the limits of the assumptions and simplifications involved in making the melt estimates, it seems reasonable to conclude that melting does make a significant contribution to the observed salinity decrease and in balancing the present rate of advance of the glacier terminus.

The sill in the narrows and the depth of the chemocline in WLB

The inflows of fresh and saline water that enter WLB, together with the level of the sill in the narrows separating ELB and WLB, control the character and position of the WLB chemocline. The sill and the chemocline in turn influence the exchange of fresh and saline water between ELB and WLB.

The position of the WLB chemocline has remained relatively stable, within the accuracy of our measurements, since 1991 (Figs. 3b,c, 4b,c, 5c,d). The coincidence of the top of the chemocline with the level of the sill implies that, except during periods of high brine inflow, the sill acts to block the flow of salty water from within and below the WLB chemocline into ELB. However, on occasion the level of the chemocline may rise sufficiently to allow some flow of chemocline water to occur over the sill into ELB where it would form a density undercurrent and eventually intrude into the main ELB chemocline at its level of neutral buoyancy. Evidence for such flow has been provided by Doran et al. (2014), who referred to "chemocline leakage" from WLB when explaining the unusual older apparent ages of saline, dissolved inorganic carbon (DIC)-rich, water, characteristic of WLB

(Poreda et al. 2004), in the ELB main chemocline between depths of 20–25 m shown in Doran et al. (2014) Fig. 4D. Our conceptual sketch in Fig. 10 includes orange arrows showing the likely path of leakage flow. Mechanisms causing the chemocline to rise, including inflows below the chemocline and glacier advance, are discussed below.

Because WLB water below the level of the sill is density stratified, inflows below sill level will form horizontal intrusions at their level of neutral density, lifting all of the water above this depth to higher levels. This process is illustrated by the vertical black arrows just below the chemocline in Fig. 10. We have described evidence for the existence of cold, saline inflows below the chemocline based on the resistivity data of Mikucki et al. (2015), the radio echo sounding data and hydraulic-potential modeling of Badgeley et al. (2017) and from examination of temperature and salinity data within the lake, although we have no way of quantifying the volumes of sub-glacial brines, or of groundwater from other sources, that enter the Lake Bonney. We have also described input of freshwater from melt below the chemocline, which seems to be of the same order as (and therefore in approximate balance with) glacier advance. These are the mechanisms that could cause the level of the WLB chemocline to rise.

Doran et al. (2014) noted that advance of the Taylor Glacier into WLB displaces volume previously occupied by lake water, thereby providing a further mechanism for raising the level of the lake and pushing water over the sill from WLB to ELB. Some of the displaced volume will be below the WLB chemocline and force the chemocline to rise. A calculation for the order of magnitude of chemocline rise can be made using the 20-yr average advance rate for the Taylor Glacier terminus of 5 m yr^{-1} deduced from Fountain et al.'s (2004, Table 5) and Pettit et al.'s (2014, Fig. 3). Approximating the shape of the exposed glacier face below the chemocline (taken as the level of 40 PSU salinity contour) as a trapezoid (as above in "Melting at the submerged glacier face" section) with top width 307 m at 15.2 m depth and height 10.8 m to the bottom at 26 m depth with bottom width 96.8 m, gives an estimate of 2180 m^2 for the frontal area of the exposed glacier face below the chemocline. Multiplying by an advance rate of 5 m yr^{-1} gives a figure for displaced volume below the chemocline of 10,900 m^3 yr^{-1}. Using a horizontal area of 7.44×10^5 m^2 (Obryk, unpubl. hypsographic data) within the depth contour at chemocline level gives an average vertical displacement for the chemocline of approximately 1.5 cm yr^{-1}, which is too small to be detected reliably in our data. A much greater volume of displacement occurs above the chemocline, where the glacier front occupies a much larger area. Using the same trapezoidal approximation referred to above, we estimate total frontal area of the glacier between 4 m and 26 m depth as 6840 m^2, implying a volume of 34,200 m^3 yr^{-1} water displaced by glacier advance. When this is spread over the entire lake area of 4.11×10^6 m^2 at 4 m depth, the resulting rise in lake level is 8 mm yr^{-1}, which is within the range of measurement error for lake level. This is not meant to imply that glacier advance occurs in a continuous or smooth fashion over time, but rather it is intended to provide rough estimates for effects of the displacement of lake water by glacier advance, and indicates that the effects on WLB chemocline rise and entire lake level rise would be barely detectable in our CTD and lake level data. The displacements calculated above are based on ice volumes; if all of the ice melted, the volumes would be reduced by factor of 0.91, the ratio of the density of ice to that of liquid water.

Fresh meltwater inflows

We expect that volumes of subsurface inflows, whether from sub-glacial brines or other sources, are small compared to those of fresh meltwater inflows from streams that occur during the austral summer and enter the lake at its surface. Lake levels tend to drop gradually from February to November when ablation exceeds inflows, and then rise more abruptly from December to January during the melt season when inflows exceed ablation (Ebnet et al. 2005; Dugan et al. 2013; Doran et al. 2014). Based on unpublished stream gaging data accessible on the McMurdo Dry Valleys Long Term Ecological Research project website (http://www.mcmlter.org/streams-data-sets), Fountain et al. (1999, their Fig. 5) and Doran et al. (2014, their Table 4), we estimate that 80–90% of the fresh meltwater input to Lake Bonney enters the lake at the western end of WLB as highly intermittent direct runoff from the Taylor Glacier itself and in streams draining from the Taylor Glacier and nearby mountain glaciers, especially the Rhone Glacier. Such flows occur only on warm days with air temperatures near or above 0°C, with significant flows generally occurring only in December and January. Assuming that the surface area of WLB accounts for approximately 23% of the total Lake Bonney surface area, and ELB for 77% (Priscu, unpubl. hypsographic data), a substantial fraction of such inflow to WLB must find its way into ELB in order to maintain hydrostatic equilibrium, implying that the net flow on average through the narrows must be from west to east.

Temperature data (Figs. 3a, 4a) suggest that there is also flow from ELB to WLB, with flow through the narrows composed of several (at least three, possibly more) layers moving in opposing directions, superimposed on the net average west-east flow. This appears to be true both for the January 1991 transect (Fig. 3a), after meltwater streams had been flowing for some time, as well as for the November 2009 transect, before lake levels began to rise (Fig. 4a). A possible scenario describing the flow structure is described below and illustrated in Fig. 10, with the salinity boundaries specified for different flow layers being somewhat subjective.

During the melt season, the uppermost flow layer immediately below the lake's ice-cover is composed of freshwater

originating from the Taylor Glacier, Rhone Glacier and associated streams, supplemented by meltwater from the submerged Taylor Glacier face, and flowing from WLB to ELB. This water eventually mixes with water below the ice in ELB and is the main source of summer rises in lake level. The lowest flow layer, just above the sill (orange arrows, Fig. 10), consists of saltier water from below the WLB chemocline that is raised above the sill by mechanisms discussed earlier in connection with chemocline leakage, as well as water within and just above the chemocline itself. We do not know whether leakage is an episodic or continuous process, although, given the observations of intermittent flows in the region, it seems likely that is episodic. Our interpolation of salinity contours in Fig. 4b (region between lake bottom and dashed line) implies that water from within the 75–35 PSU contours overflows the sill as a west-to-east flow along the bottom through the narrows, continuing down the slope as a density current in ELB until it reaches its level of neutral buoyancy, where it intrudes horizontally within the ELB chemocline, probably over a range of salinities. Water from upper levels of the WLB chemocline, between the 35–20 PSU contours, also forms part of the west-east flow over the sill, but has mixed with fresher water above the chemocline in WLB and is probably the source of the "shoulder" that is characteristic of salinity and density profiles in ELB (Fig. 8b, 2009 salinities between 25 and 30 PSU; see also wider gap in corresponding ELB salinity contours, Fig. 3b). Spigel and Priscu (1998) suggested that the west-east flow in the upper levels of the chemocline helps preserve the sharpness of the WLB chemocline gradient by continually transporting water from the upper chemocline into ELB and offsetting effects of diffusion. No such mechanism exists in ELB, where the chemocline shape appears to be controlled mainly by diffusion. We note that salinity in the "shoulder" on the ELB chemocline has increased by approximately 2 PSU from January 1991 to November 2009, accompanying a general increase in salinity between the bottom of the ice and the chemocline over this period in both lobes that diminishes as the ice cover is approached. Based on the 2009 ELB profile at site NR8, it also appears that salinities have decreased slightly within and below the deeper part of the main ELB chemocline, possibly due to diffusion and contributing to the increase in salinity in the "shoulder" on top of the ELB chemocline. A salt balance similar to that described for WLB indicates TDS concentration in the "shoulder" between elevations 45.557 mASL and 49.025 mASL (volume 6.60×10^6 m^3) increased at an annual average rate over the 19 yr between the profiles in Fig. 8b of 0.189 kg salt m^{-3} yr^{-1}. The net flux of salt by molecular diffusion, estimated from local TDS gradients and lake areas at the bottom and top of the "shoulder," using a molecular diffusivity of 6.90×10^{-10} m^2 s^{-1} (Robinson and Stokes 1955; Weast 1976) was 0.069 kg salt m^{-3} yr^{-1}, and so cannot account for the entire increase. We assume that the deficit is made up by flow from the top of the WLB chemocline. Use of a turbulent diffusivity would increase the estimated contribution by diffusion. However, on the basis of temperature and conductivity microstructure profiling, Spigel and Priscu (1998) concluded that there was no evidence of turbulence in the ELB chemocline, so we do not think there is any basis for using a larger value of diffusivity.

In between the uppermost flow layer directly under the ice, and lower flow layers on top of the WLB chemocline, are one or more layers that appear to transport water from ELB to WLB, as reflected by the tongues of warmer water from ELB as seen in Figs. 3a, 4a. The suggested multi-layered exchange flow through the narrows may be partly driven by small density differences between water in ELB and WLB above sill level, but it may also be associated with melting of freshwater from the face of the Taylor Glacier that generates a circulation drawing water from ELB through the narrows toward the glacier. As discussed in "Melting at the submerged glacier face" section, such a circulation could be generated by melting at the face of the glacier in the relatively freshwater above the chemocline. We know from thermistor strings and a recently deployed profiler (unpublished data) that the temperature structure in the lake remains relatively constant throughout the year, so circulation induced by melting at the submerged part glacier face described above could supply meltwater from the glacier face to a west-east flow beneath the ice cover on a year-round basis.

References

Armitage, K. B., and H. B. House. 1962. A limnological reconnaissance in the area of McMurdo Sound, Antarctica. Limnol. Oceanogr. **7**: 36–41. doi:10.4319/lo.1962.7.1.0036

Badgeley, J. A., E. C. Pettit, C. G. Carr, S. Tulaczyk, J. A. Mikucki, W. B. Lyons, and MIDGE Science Team. 2017. An englacial hydrologic system of brine within a cold glacier: Blood Falls, McMurdo Dry Valleys, Antarctica. J. Glaciol. **63**: 387–400. doi:10.1017/jog.2017.16

Bendell, M. S., and B. Gebhart. 1976. Heat transfer and ice-melting in ambient water near its density extremum. Int. J. Heat Mass Transfer. **19**: 1081–1087. doi:10.1016/0017-9310(76)90138-1

Bowman, J. S., T. J. Vick-Major, R. Morgan-Kiss, C. Takacs-Vesvach, H. W. Duclow, and J. C. Priscu. 2016. Microbial community dynamics in the two polar extremes: The lakes of the McMurdo dry valleys and the West Antarctic Peninsula marine ecosystems. BioScience **66**: 829–847. doi:10.1093/biosci/biw103

Caldwell, D. R. 1978. The maximum density points of pure and saline water. Deep-Sea Res. **25**: 175–181. doi:10.1016/0146-6291(78)90005-X

Doherty, B. T., and D. R. Kester. 1974. Freezing point of seawater. J. Mar. Res. **32**: 285–300.

Doran, P. T., F. Kenig, J. L. Knoepfle, and W. B. Lyons. 2014. Radiocarbon distribution and the effect of legacy in lakes

of the McMurdo Dry Valleys, Antarctica. Limnol. Oceanogr. **59**: 811–826. doi:10.4319/lo.2014.59.3.0811

Dugan, H. A., M. K. Obryk, and P. T. Doran. 2013. Lake ice ablation rates from permanently ice-covered Antarctic lakes. J. Glaciol. **59**: 491–498. doi:10.3189/2013JoG12J080

Ebnet, A. F., A. G. Fountain, T. H. Nylen, D. M. McKnight, and C. L. Jaros. 2005. A temperature-index model of stream flow at below-freezing temperatures in Taylor Valley, Antarctica. Ann. Glaciol. **40**: 76–82. doi:10.3189/172756405781813519

Fofonoff, N. P., and R. C. Millard, Jr. 1983. Algorithms for computation of fundamental properties of seawater, 53 p. UNESCO Technical Papers in Marine Science 44. Division of Marine Sciences, UNESCO.

Fountain, A. G., and others. 1999. Physical controls on the Taylor Valley ecosystem, Antarctica. BioScience **49**: 961–971. doi:10.1525/bisi.1999.49.12.961

Fountain, A. G., T. A. Neumann, P. L. Glenn, and T. Chinn. 2004. Can climate warming induce glacier advance in Taylor Valley, Antarctica? J. Glaciol. **50**: 556–564. doi:10.3189/172756504781829701

Gayen, B., R. W. Griffiths, and R. C. Kerr. 2015. Melting driven convection at the ice-water interface. Procedia IUTAM **15**: 78–85. doi:10.1016/j.piutam.2015.04.012

Golden Software. 2012. Surfer 11 users guide, p. 1032. Golden Software.

Hendy, C. H., A. T. Wilson, and K. B. Popplewell. and D.A. House. 1977. Dating of geochemical events in Lake Bonney, Antarctica, and their relation to glacial and climate changes. N. Z. J. Geol. Geophys. **20**: 1103–1122. doi:10.1080/00288306.1977.10420698

Huppert, H. E., and J. S. Turner. 1978. On melting icebergs. Nature **271**: 46–48. doi:10.1038/271046a0

Huppert, H. E., and E. G. Josberger. 1980. The melting of ice in cold stratified water. J. Phys. Oceanogr. **10**: 953–960. doi:10.1175/1520-0485(1980)010<0953:TMOIIC>2.0.CO;2

Huppert, H. E., and J. S. Turner. 1980. Ice blocks melting into a salinity gradient. J. Fluid Mech. **100**: 367–384. doi:10.1017/S0022112080001206

Huppert, H. E., and J. S. Turner. 1981. Double-diffusive convection. J. Fluid Mech. **106**: 299–329. doi:10.1017/S0022112081001614

Jacobs, S. S., H. E. Huppert, G. Holdsworth, and D. J. Drewry. 1981. Thermohaline steps induced by melting of the Erebus Glacier Tongue. J. Geophys. Res. **86**: 6547–6555. doi:10.1029/JC086iC07p06547

Jeevaraj, C. V., and J. Imberger. 1991. Experimental study of double-diffusive instability in sidewall heating. J. Fluid Mech. **222**: 565–586. doi:10.1017/S0022112091001222

Josberger, E. G., and S. Martin. 1981. A laboratory and theoretical study of the boundary layer adjacent to a vertical melting ice wall in salt water. J. Fluid Mech. **111**: 439–473. doi:10.1017/S0022112081002450

Kirk, J. T. O. 1994. Light and photosynthesis in aquatic ecosystems, 2nd ed. Cambridge Univ. Press.

Lide, D. R. [ed.]. 2005. CRC handbook of chemistry and physics, 86th ed. CRC Press.

Lizotte, M. P., and J. C. Priscu. 1992. Spectral irradiance and bio-optical properties in perennially ice-covered lakes of the Dry Valleys (McMurdo Sound, Antarctica), p. 1–14. *In* D. H. Elliott [ed.], Contributions to Antarctic research III. Antarctic research series, v. 57. American Geophysical Union. doi:10.1029/AR057p0001

Lyons, W. B., C. Dowling, K. A. Welch, G. Synder, R. J. Poreda, P. T. Doran, and A. Fountain. 2005. Dating water and solute additions to ice-covered Antarctic lakes. Geochim. Cosmochim. Acta **69**: A720. http://www.uta.edu/ees/faculty/hu/assets/researchPDF/2005%20Goldschmidt%20iodine.pdf

MacIntyre, S., J. O. Sickman, S. A. Goldthwait, and G. W. Kling. 2006. Physical pathways of nutrient supply in a small oligotrophic arctic lake during summer stratification. Limnol. Oceanogr. **51**: 1107–1124. doi:10.4319/lo.2006.51.2.1107

Malki-Epshtein, L., O. M. Phillips, and H. E. Huppert. 2004. The growth and structure of double-diffusive cells adjacent to a cooled sidewall in a salt-stratified environment. J. Fluid Mech. **518**: 347–362. doi:10.1017/S0022112004001235

Mikucki, J. A., C. M. Foreman, B. Sattler, W. B. Lyons, and J. C. Priscu. 2004. Geomicrobiology of Blood Falls: An iron-rich saline discharge at the terminus of the Taylor Glacier, Antarctica. Aquat. Geochem. **10**: 199–220. doi:10.1007/s10498-004-2259-x

Mikucki, J. A., and J. C. Priscu. 2007. Bacterial diversity associated with Blood Falls, a subglacial outflow from the Taylor Glacier, Antarctica. Appl. Environ. Microbiol. **73**: 4029–4039. doi:10.1128/AEM.01396-06

Mikucki, J. A., and others. 2009. A contemporary microbially maintained subglacial ferrous "ocean". Science **324**: 397–400. doi:10.1126/science.1167350

Mikucki, J. A., and others. 2015. Deep groundwater and potential subsurface habitats beneath an Antarctic dry valley. Nat. Commun. **6**: 6831. doi:10.1038/ncomms7831

Millero, F. L., and W. H. Leung. 1976. The thermodynamics of seawater at one atmosphere. Am. J. Sci. **276**: 1035–1077. doi:10.2475/ajs.276.9.1035

Obryk, M. K., P. T. Doran, and J. C. Priscu. 2014. The permanent ice cover of Lake Bonney, Antarctica: The influence of thickness and sediment distribution on photosynthetically available radiation and chlorophyll-a distribution in the underlying water column. J. Geophys. Res. Biogeosci. **119**: 1879. doi:10.1002/2014JG002672

Obryk, M. K., and others. 2016. Responses of Antarctic marine and freshwater ecosystems to changing ice conditions. Bioscience **66**: 864–879. doi:10.1093/biosci/biw109

Oshima, K. I., T. Kawamura, T. Takizawa, and S. Ushio. 1994. Step-like structure in temperature and salinity

profiles observed near icebergs trapped in fast ice, Antarctica. J. Oceanogr. **50**: 365–372. doi:10.1007/BF02239522

Pettit, E. C., E. N. Whorton, E. D. Waddington, and R. S. Sletten. 2014. Influence of debris-rich basal ice on flow of a polar glacier. J. Glaciol. **60**: 989–1006. doi:10.3189/2014JoG13J161

Phillips, O. M. 1966. The dynamics of the upper ocean. Cambridge Univ. Press.

Pond, S., and G. L. Pickard. 1978. Introductory dynamic oceanography. Pergamon Press.

Poreda, R. J., A. G. Hunt, W. B. Lyons, and K. A. Welch. 2004. The helium isotope chemistry of Lake Bonney, Taylor Valley, Antarctica: Timing of late Holocene climate change in Antarctica. Aquat. Geochem. **10**: 353–371. doi:10.1007/s10498-004-2265-z

Ramires, M. L. V., C. A. N. de Castro, Y. Nagasaka, A. Nagashima, M. J. Assael, and W. A. Wakeham. 1995. Standard reference data for the thermal conductivity of water. J. Phys. Chem. Ref. Data **24**: 1377–1381. doi:10.1063/1.555963

Robinson, R. A., and R. H. Stokes. 1955. Electrolyte solutions. Butterworth Scientific.

Schladow, S. G., E. Thomas, and J. R. Koseff. 1992. The dynamics of intrusions into a thermohaline stratification. J. Fluid Mech. **236**: 127–165. doi:10.1017/S002211209200137X

Schneider, W. 1981. Flow induced by jets and plumes. J. Fluid Mech. **108**: 55–65. doi:10.1017/S0022112081001985

Spigel, R. H., and J. C. Priscu. 1996. Evolution of temperature and salt structure of Lake Bonney, a chemically stratified Antarctic lake. Hydrobiologia **321**: 177–190. doi:10.1007/BF00143749

Spigel, R. H., and J. C. Priscu. 1998. Physical limnology of the McMurdo Dry Valley lakes, p. 153–187. *In* J. C. Priscu [ed.], Ecosystem dynamics in a polar desert. The McMurdo Dry Valleys, Antarctica. Antarctic research series, v. 72. American Geophysical Union.

Stephenson, Jr., G. R., J. Sprintall, S. T. Gille, M. Vernet, J. J. Helly, and R. S. Kaufman. 2011. Subsurface melting of a free-floating Antarctic iceberg. Deep-Sea Res. Part II Top. Stud. Oceanogr. **58**: 1336–1345. doi:10.1016/j.dsr2.2010.11.009

Stone, W., and others. 2010. Design and deployment of a four-degrees-of-freedom hovering autonomous underwater vehicle for sub-ice exploration and mapping. J. Eng. Mar. Environ. **224**: 341–361. doi:10.1243/14750902JEME214

Turner, J. S. 1978. Double-diffusive intrusions into a density gradient. J. Geophys. Res. **83**: 2887–2901.

Weast, R. C. [ed.]. 1976. CRC handbook of chemistry and physics, 57th ed. CRC Press.

Winslow, L. A., H. A. Dugan, H. N. Buelow, K. D. Cronin, J. C. Priscu, C. Takaccs-Vesbach, and P. T. Doran. 2014. Autonomous year-round sampling and sensing to explore the physical and biological habitability of permanently ice-covered Antarctic lakes. Mar. Technol. Soc. J. **48**: 9–17. doi:10.4031/MTSJ.48.5.6

Acknowledgments

We would like to thank everyone in the ENDURANCE teams and the LTER lake teams for making this project successful. This project was largely supported by a grant from the NASA Astrobiology Science and Technology for Exploring Planets (ASTEP) program (#NNX07AM88G). The National Science Foundation, Office of Polar Programs, provided logistical support in the field, and funding for the McMurdo Long Term Ecological Research (LTER) site which supplied contextual and long term data to this project (grant numbers 9810219, 0096250, 0832755, 1041742, and 1115245).

Conflict of Interest

None declared.

Submitted 24 March 2017
Revised 29 September 2017
Accepted 14 November 2017

Associate editor: Francisco Rueda